*Earthquake Geotechnical Engineering for Protection and Development of Environment and Constructions – Silvestri & Moraci (Eds)*
*© 2019 Associazione Geotecnica Italiana, Rome, Italy, ISBN 978-0-367-14328-2*

# A multidisciplinary approach for the seismic characterization of the Cassino plain (central Italy)

M. Saroli
*Università degli Studi di Cassino e del Lazio Meridionale, Cassino, Italy*

M. Albano, G. Milana & M. Moro
*Istituto Nazionale di Geofisica e Vulcanologia, Roma, Italy*

G. Modoni, R.L. Spacagna & P. Croce
*Università degli Studi di Cassino e del Lazio Meridionale, Cassino, Italy*

S. Stramondo & C. Tolomei
*Istituto Nazionale di Geofisica e Vulcanologia, Roma, Italy*

ABSTRACT: Thanks to its geological, hydrogeological and historical features, the Cassino basin is one of the most important areas of central Italy. More than two hundred soil borings, some of them reaching depths as high as 100 m, have revealed a subsoil characterized by a calcareous platform and post-orogenetic series forming a tectonic basin filled by lacustrine and volcanic deposits. Together with the borehole data, a series of microtremor measurements have been performed to estimate the natural frequency of oscillation of the more deformable deposits to study at a very detailed scale the seismic response of the site. The combination of geophysical data with the information given by the deep boreholes, permitted to rebuild the geological complexities of the tectonically driven seismic bedrock, outcropping continuously at east and west of the basin. This study forms the basis for numerical analyses aimed at predicting the unknown local amplification effects.

## 1 INTRODUCTION

The central Apennines of the Italian territory are one of the most seismically active areas in the Mediterranean province, as highlighted by the occurrence of strong earthquakes in the past and by the presence of a large number of active faults (Rovida et al. 2016). Faults play a primary role in shaping the landscape of the mountain chain. Indeed, the present active extensional tectonics controls the development of many intermontane basins bounded by seismogenic normal faults and filled by sedimentary soils. Such areas, characterized by flat or gently sloping topography, favored the development of critical historical settlements in the past and promoted dense urbanization in recent times. The closeness of these developments to active, seismogenic faults is the basis of high exposure to seismic risk for industrial centers, cultural heritage sites, and thousands of people. Indeed, many of the recent earthquakes in Italy caused severe damages and life loss (Tertulliani et al. 2011, Galli et al. 2012, 2017).

The Cassino town (Figure 1) is as an example of middle size Italian urban settlements located in an intermontane basin. The town presents peculiar socio-economical, historical, environmental, geological and hydrogeological features (Saroli et al. 2014, Lancia et al. 2018). During the Second World War, the city was completely destroyed. Since then, Cassino has been rebuilt, and the population has increased from about twenty to forty thousand people in less than 20 years. Over this period, the urban area has considerably expanded over the alluvial plain at the foot of the Montecassino hill. The town hosts a University and strategic infrastructures such as the Campania aqueduct, and the Busso-Paliano methane pipeline.

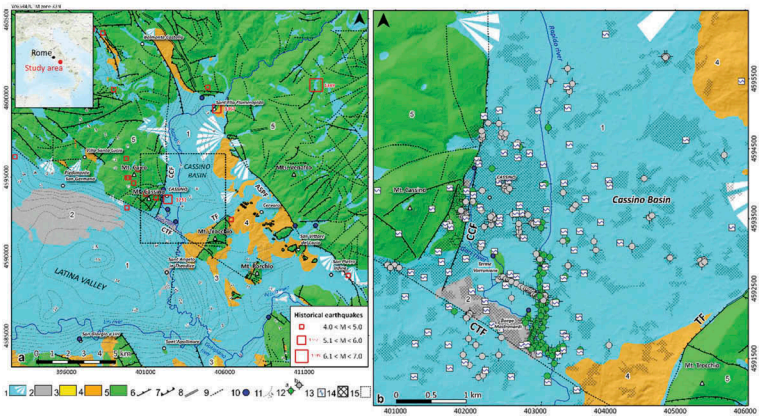


Figure 1. Geological and structural map of the end sector of the Latina Valley, highlighting the main features of the fault system at the surface and the outcropping pre-Quaternary and Quaternary deposits, modified from Saroli et al. (2014). Key to the legend: 1) Recent and old debris, debris fans, eluvial, colluvial and lacustrine soils (Middle Pleistocene - Holocene); 2) Travertine (Middle Pleistocene - Upper Pleistocene); 3) gravels and sands (Messinian - Lower Pliocene); 4) sandstones and grey clays (flysch) (Upper Tortonian); 5) Limestones and dolostones with emipelagic marls (Lias - Lower Tortonian); 6) Normal faults; 7) Thrusts; 8) Strike-slip faults; 9) Inferred/buried faults; 10) Springs; 11) Isolines of the residual Bouguer anomalies (mGal) from Amadei et al. (1978); 12) Boreholes reaching (a) and not reaching (b) the carbonate bedrock; 13) Microtremor measurements; 14) Urban area footprint; 15) Detail of the study area in Figure 1b. Historical M > 5 earthquakes with the year of the event are taken from the parametric catalog of Italian earthquakes (Rovida et al. 2016).

The seismic analysis, based on historical and instrumental data (Rovida et al. 2016), shows that the Cassino basin has been affected by strong earthquakes in the past (e.g., San Vittore del Lazio-San Pietro Infine -Venafro, 1349; Casalvieri, 1654) with estimated magnitudes ranging between 6.1 and 6.7 (Figure 1a) and macroseismic intensity reaching grade 10. It is therefore mandatory to understand and mitigate the seismic risk of the area. Among others, essential elements that may help to mitigate the seismic risk for sustainable use of the territory are a detailed study of the seismic behavior of neighboring active normal faults and a deep understanding of the peculiar geological features of the area. Despite we sufficiently know the regional seismic hazard of the area, a thorough understanding of the local geological and geotechnical characteristics of the Quaternary soils filling the Cassino basin and their impact on seismic ground motions and local amplifications has not been afforded yet. In this work, we shed light on the geometrical features and dynamic properties of the soils filling the Cassino basin. Such knowledge represents one of the key pillars for the quantification of the seismic hazard and the mitigation of the seismic risk of the area.

## 2 GEOLOGICAL AND TECTONIC SETTING

The Cassino town is located in a plio-pleistocenic intermontane basin at the southeastern sector of the Latina Valley, a broad and narrow depression with a northwest-southeast trend, developed since the Neogene along the Apennines thrust and fold orogenic belt (Figure 1a). The basin has a graben structure, striking northeast-southwest with the depocenter shifted toward the north. This structure was inherited from a late extensional tectonic phase, superposed on a fold and thrust geometry derived from a previous contractional period. Normal faults are evident along the whole area, hiding transpressive and compressive elements (Saroli et al. 2014). The main tectonic feature of the region is the Atina-San Pietro active fault (ASPF in Figure 1a) (Saroli & Moro 2012) to the northeast. This fault, with an estimated slip rate of approximately 0.3–0.5 mm/a, shows tectonic evidence since the Lias age (Saroli et al. 2014). The Caira–Cassino

fault to the west (CCF) and the Trocchio fault (TF) to the east, outline the horst-and-graben structure of the basin, with the limestone outcrops of *Terme Varroniane* and *Borgo Mastronardi* representing two horsts of this system (Figure 1b), as confirmed by geological and hydrogeological evidence (Saroli et al. 2016, Lancia et al. 2018). Finally, the Cassino-Trocchio fault (CTF) dissects the plain to the south, downthrowing the southwestern sector of the Latina Valley. Such a robust tectonic control and the amount of the associated deformations produced a profound disarticulation of the carbonatic substratum, whose depth varies between few tens of meters close to the carbonate ridges, up to several hundred meters in the northeastern part of the plain (Boni et al. 1982). The typical lithostratigraphic sequence starts with approximately 2000 m of dolostones and limestones belonging to the Latium-Abruzzi carbonate platform, followed by ramp limestones and emipelagic marls (5 in Figure 1a) which outcrop close to the Cassino town and along the ASPF fault. The sedimentary platform is then covered by tortonian post-collisional arenaceous and clayey deposits with an epi-continental and continental origin (4 in Figure 1a), followed by piggyback sequences formed during the thrust-system development (3 in Figure 1a). The following plio-pleistocenic filling has an epicontinental and continental origin with loose gravel, loose sands and pudding stones on the bottom of a lacustrine series (1 in Figure 1a). The lacustrine environment is due to the Roccamonfina volcanic edifice construction and the subsequent obstruction of the Latina Valley (Devoto 1965). The thickness of the lacustrine deposit is extraordinarily uneven and can reach more than 100 meters. Thin levels of raven ashes are commonly present in the lacustrine body, due to the interaction between paleo-Lirino Lake and the Roccamonfina and Campi Flegrei volcanic activity. Indeed, in the eastern part of the basin, there is a diffused outcropping of tuff. Travertine plateaus (2 in Figure 1a) and marsh silt mark the complete filling of the basin, on the top of the Lirino-series. Last volcanic events occur in a continental-fluvial environment and give origin to reshuffle volcanic sands interdigitated with detrital inputs. In the end, Upper-Pleistocene-Holocene, fluvial environment (Rapido, Liri and Gari Rivers) has incised and covered the lacustrine sequence with 5–15 m of alluvial silt, sand, and gravel. Nearby calcareous bedrock, colluvial soils, and alluvial fans can hide the relationship between calcareous bedrock and Quaternary deposits.

## 3 DATA AND METHODS

The available dataset includes deep and shallow boreholes, and in situ geophysical tests, the latter including single station microtremor measurements, and a large number of laboratory tests. All these data were combined in a specially devised Geographical Information System (GIS) to estimate the buried geometry of the basin and the dynamic features of the loose sedimentary soils using geostatistical techniques.

### 3.1 *Borehole data*

Unpublished data for 219 boreholes were collected from the municipal archive and the available literature (Figure 1b). Among them, 83 boreholes were drilled down to the pre-Quaternary arenaceous and sedimentary bedrock for oil research and groundwater exploitation, thus providing significant insights about the morphology and the thickness of Quaternary deposits (Saroli et al. 2014). The other 136 shallow boreholes provided information about the geotechnical properties of the Quaternary soft deposits, i.e., the state, elastic, hydraulic, and strength parameters.

### 3.2 *Microtremor surveys*

A campaign of systematic surveys aimed at the seismic microzonation of the municipality of Cassino has been undertaken in the period 2008-2009 and 2011, respectively. In the first campaign (2008-2009), microtremors were recorded at 73 sites, mainly located in the urban area of the Cassino town (Figure 1b). The recording length was approximately 30 minutes, which is recommended for spectral analysis at least down to 0.5 Hz (SESAME 2004, Molnar et al. 2018). In the second campaign (2011), further 27 measurements were performed with a recording

length of approximately 20 minutes. Microtremor acquisitions in the urban environment of the Cassino town presented significant challenges since transient signals, such as road traffic and machinery, impact on quality of measurements. Therefore, recordings were performed at a distance of more than 10 meters from infrastructures and at different times of the day and even at night to improve the reliability of the recorded signals (Molnar et al. 2018). Recordings at a site were repeated in case of inconsistency with the results of neighboring measurements.

Microtremor recordings were processed according to the horizontal-to-vertical spectral ratio method (from now on MHVSR) (Nakamura 1989) for retrieval and evaluation of the site period or fundamental frequency of unconsolidated sediments over high-velocity bedrock. The method calculates the ratio of the horizontal-to-vertical Fourier spectra derived from microtremor recordings of a three-component sensor. In this study, the MHVSR analysis was carried out using the open source software Geopsy (www.geopsy.org). Recorded time series were visually inspected to identify possible erroneous measurements and stronger transient noise. All the three spatial components of the recorded time history were divided into non-overlapping windows of 40 seconds. Amplitude spectra were computed in the frequency range of 0.25–20Hz with the fast Fourier transform and using a triangular window with 5% tapering. The Fourier spectra were smoothed by the Konno–Ohmachi function with a bandwidth coefficient b=40. MHVSR was then computed for each window as the geometric average of both horizontal component spectra divided by the vertical spectrum. Finally, we calculated the mean spectral amplitude for the three components and the mean MHVSR. A directional MHVSR analysis was also performed in 10° angular steps to identify the possible directions of the noise sources. The latter was analyzed by estimating the HVSR curves derived by projecting the ground motion along different horizontal directions. Some measurements were disregarded because of recording problems in one of the three components of the noise. Sharp peaks on all single-component spectra also affected most of the measurements at frequencies of approximately 1.5 Hz and 5 Hz, respectively. These peaks show a strong directionality and, in some cases, mask the resonant frequency of the site on the MHVSR curve, thus making the measurement useless. The nature of the peaks is clearly of industrial origin since some measurements, repeated during the night at the same locations, did not show anomalous frequency peaks. For each of the remaining H/V curves, we assessed the presence of one or more resonant peaks fulfilling the criteria of reliability and clarity defined by the SESAME working group (SESAME 2004).

## 4 RESULTS AND DISCUSSION

### 4.1 *Classification and interpretation of borehole logs*

The analysis of the deep boreholes allowed a first reconstruction of the carbonate basement and the relationship between carbonates, sandstones, gravels and sands, and Quaternary deposits. The depth of the carbonate basement (colored circles in Figure 2a) is hugely uneven. The investigated depths vary from a few meters close to the carbonate outcrops to more than 300 meters towards southwest and northeast of the plain. In some areas, the depth variation is abrupt, indicating the presence of several buried faults. From northwest to southeast, a first sudden change of the carbonate depth is carried out by the CCF fault, which significantly dissects the carbonates up to 100 meters, as testified by the boreholes A-C in Figure 2b. Slightly to the south, the archaic horst-and-graben structure is preserved with the outcropping horsts of *Terme Varrionane* and *Borgo Mastronardi* and the grabens reaching 90-meter depth (boreholes D-E in Figure 2b). A third horst is identified at the confluence of the Gari and Rapido rivers to the southeast (boreholes F-G in Figure 2b) as confirmed by the presence of previously unmapped springs (Saroli et al. 2014). Quaternary lacustrine and fluvial deposits lay directly on the carbonates (boreholes A-G in Figure 2b) over the area bordered by the white dashed line in Figure 2a. However, banks of gravels and sands up to 30 m thick sometimes are found between the lacustrine sequence and the Mesozoic–Cenozoic bedrock (boreholes D and E). These banks are identified in the graben between the *Terme Varroniane* and *Borgo Mastronardi* horsts (circles with an orange outline in Figure 2a) (Saroli et al. 2014). To the northeast, the carbonate depth increases from 50 to more than 300 meters (boreholes H-K in Figure 2b),

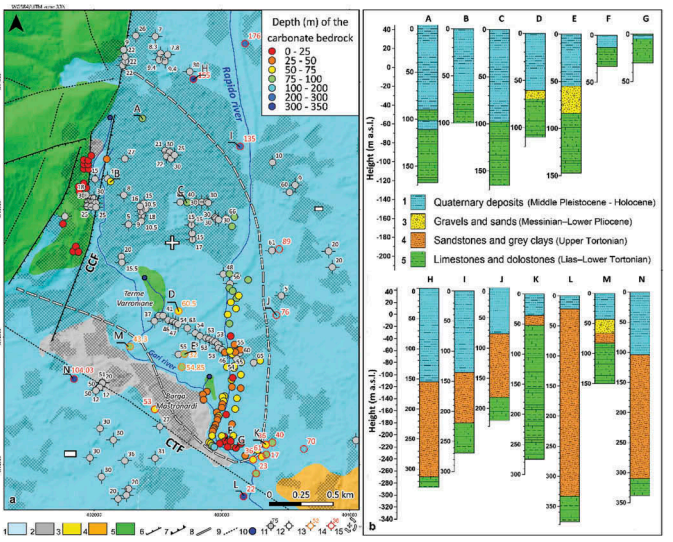


Figure 2. Analysis of the available boreholes on the Cassino basin. Key to the legend: from 1 to 10 refer to the caption of Figure 1; 11) Boreholes intercepting Quaternary deposits only (the numbers identify the borehole depth); 12) Boreholes intercepting Quaternary deposits (1), and the carbonatic substratum (5) (the color palette indicates the depth of the carbonatic substratum); 13) Boreholes intercepting Quaternary deposits (1), gravels and sands (3), and the carbonatic substratum (5) (the orange number identifies the roof depth of gravels and sands); 14) Boreholes intercepting Quaternary deposits (1), sandstones and grey clays (4), and the carbonatic substratum (5) (the red number identifies the roof depth of the sandstones and grey clays); 15) Presumed boundary line between the carbonatic bedrock (plus symbol) and arenaceous bedrock (minus symbol), below the Quaternary sediments.

giving way to sandstones and gray clays (circles with a red outline in Figure 2a), which widely outcrop to the northeast and southeast of the Cassino plain (Figure 1a). The Quaternary deposits lay directly on the Tortonian sandstones and reach depths of approximately 150-180 meters (borehole H in Figure 2b), because of the activity of the ASPF fault. To the south of the *Terme Varroniane* and *Borgo Mastronardi* outcrops, the intense action of the CTF fault is testified by boreholes L, M and N. Indeed, the carbonate bedrock sinks from approximately 80 meters (borehole M) to more than 300 meters (boreholes L and N) in less than 250-meter distance. Even in this area, Quaternary deposits cover sandstones and gray clays with an investigated thickness of more than 300m (borehole L), sometimes interspersed by gravels and sands (borehole M). Therefore, the area inside the dashed white line in Figure 2a presents a bedrock composed predominantly by limestones and dolostones (5) and results on a structural high (plus symbol in Figure 2a) respect to the rest of the basin (minus symbol in Figure 2a) where the bedrock is constituted mainly by sandstones and grey clays (4).

## 4.2 *Microtremor results*

The computed MHVSR curves were grouped into three classes according to the principal outcropping lithologies in the Cassino basin (layers 1, 4 and 5 in Figure 1a). Measurements performed on limestones and dolostones (layer 5) (Figure 3a) show some broad high-frequency peaks that depend on the degree of fractures opening and geomorphic and structural complexities (Pagliaroli et al. 2015). Measurements performed on the sandstones and grey clays (layer 4) (Figure 3b) are also flat, thus testifying the absence of a strong impedance contrast at the contact between layer 4 and 5. Therefore, layers 4 and 5 are assumed as a seismic bedrock.

Measurements on the fluviolacustrine soils (layer 1) were grouped according to the distance from the outcropping bedrock (from now on DOB), defined as the lowest distance between the measurement point and the outcrops of layers 4 and layer 5. The retrieved frequency peaks are

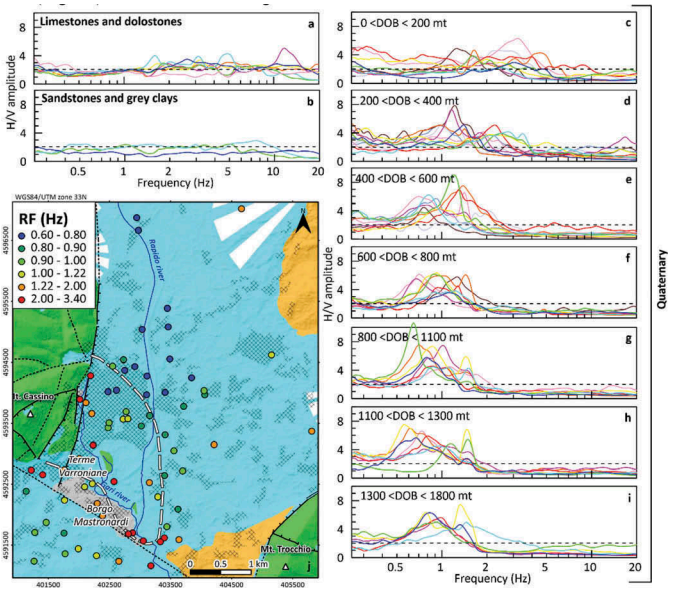


Figure 3. Results of the MHVSR processing and the exploratory spatial analysis of the RFs. a) H/V curves of microtremor measurements performed on limestones and dolostones (layer 5). b) H/V curves of microtremor measurements performed on sandstones and grey clays (layer 4). c-i) H/V curves of microtremor measurements performed on the Quaternary layer (layer 1), classified according to the DOB. j) Classed post map of RF values estimated for the measurements performed on the Quaternary layer (layer 1) (classes according to quantile classification).

generally bright and often sharp. Thus, they were interpreted as the resonant frequencies (from now on RF) of the site. Measurements not fulfilling the SESAME criteria were disregarded, however, some of them were considered as relevant RF since they were consistent with those at closest locations. MHVSR curves show significant frequency peaks over the range 0.6-3.4 Hz (Figure 3c–j). For small DOB, peak frequencies are broad and span a broad range of frequencies because of deviations from the assumption of 1D stratigraphy. For higher DOB, frequency peaks are narrower and shift towards lower frequencies, according to the observed increase of the bedrock depth towards the center of the basin (Figure 2a). The spatial distribution of the RF values (Figure 3j) shows a strong correlation with the morphology of the basin depicted in Figure 2a. RFs in the range 2–3.4 Hz result near the *Terme Varroniane* and *Borgo Mastronardi* outcrops and the Mt. Cassino hills, testifying the presence of a shallow impedance contrast. RFs gradually decrease going away from the rocky outcrops to the northwest and southeast, with the lowest values of 0.6-0.8 Hz observed at the center of the plain. A general agreement is observed between the thickness of the Quaternary layer and the RFs, with low/high RF values corresponding to the thick/thin Quaternary layer. Such a finding suggests that the seismic bedrock resembles with the contact between the Quaternary soils (layer 1) and, alternatively, the layers n° 3, 4 and 5 (Figure 1a). These three lithologies can be considered as seismic bedrock.

### 4.3 *Geostatistical analysis of MHVSR curves and correlation with borehole data*

The MHVSR RFs carried out on the Quaternary layer were interpolated using a geostatistical approach. A preliminary exploratory spatial analysis of the data (not shown) allowed discarding measures affected by anthropic noise, thus reducing the dataset to from 100 to 66 samples. To improve the interpolation, we worked with resonance periods (RP) instead of RF (Trevisani et al. 2017). We also introduced the dependency between the RFs (or RPs) and the DOB observed in Figure 3 by using the Kriging with external drift (KD) interpolation technique (Oliver & Webster 2014) and using the DOB as an auxiliary variable. Consequently, the

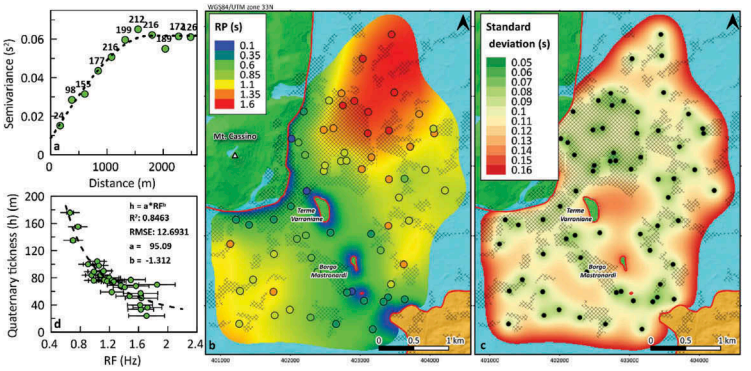


Figure 4. Geostatistical interpolation of the available RP values. a) experimental omnidirectional variogram of the RP residuals and best fit spherical model (black line). b) interpolated map of RP via KD. c) KD prediction standard deviation map of RP; d) relationship between RF from interpolated RP map (panel b) and Quaternary thickness (h) from boreholes.

explorative spatial continuity analysis of the data and the fitting of a variogram model, have been conducted on data residuals respect to a trend map. The experimental variogram has been analyzed using both variogram cloud, variogram map, directional and omnidirectional variograms, showing the absence of anisotropies, local outliers, or other patterns related to non-stationarity. The final isotropic experimental variogram (Figure 4a) has been fitted with an isotropic spherical plus nugget model (Oliver & Webster 2014). The resulting RP map is shown in Figure 4b, together with the standard error of the prediction (Figure 4c). The RP map is blanked on the areas where the prediction variance is larger than the third quantile of the variance distribution (0.0263 $s^2$), corresponding to a standard error of 0.162 s (Figure 4c). Such a choice is subjective and depends on the intended use of the interpolated map. It can be acceptable for a first-order regional scale analysis, but it is inappropriate for local scale studies. Finally, the interpolated RP values (Figure 4b) were converted to RFs and sampled in correspondence of each borehole reaching the seismic bedrock (Figure 2a). RF values with a standard deviation higher than 0.2 Hz were disregarded. The resulting plot (Figure 4d) shows that RFs are inversely proportional to the thickness of the Quaternary layer (h). Significant uncertainties in the RF values are observed for higher frequencies, i.e., for lower Quaternary thickness. The monotonic relationship between the Quaternary thickness and the RF has been defined by best fitting the experimental data with the power law relation (Ibs-von Seht & Wohlenberg 1999):

$$h = a \cdot RF^b \tag{1}$$

The coefficients a and b of the regression law are reported in Figure 4d. The estimated RF-h curve is representative of Quaternary thickness ranging between 30 and 180 meters, and it is typical of shallow-to-medium depth Quaternary basins (Gosar & Lenart 2010, Bignardi 2017).

## 5 CONCLUSIONS AND FUTURE WORK

The study performed on the Cassino basin identified the relationship between Quaternary soft deposits and the underlain hard basement, highlighting the complex shape of the bedrock and the strong variability of the thickness of Quaternary deposits. The microtremor measurements identified an impedance contrast at frequencies compatible with the contact at depth between Quaternary deposits and, alternatively, gravels and sands, sandstones and grey clays, and limestones and dolostones. Such a result shows that the microtremor method, togheter with borehole data, can be used as a complementary tool for mapping the thickness of unconsolidated sediments also in areas characterized by articulated bedrock and lithologically heterogeneous

sedimentary fill. As the input data are always to some extent uncertain, it is essential to have a sufficiently large number of measurements to improve the accuracy of the results. For this purpose, the geostatistical analysis of the MHVSR frequency peaks associates an uncertainty to the obtained map, thus identifying areas where further measurements are needed to improve the quality of the results. Future work will be devoted to the improvement of the results with other geophysical surveys such as shear-wave velocity measurements and further HVSR measures, extending the noise acquisition time to improve the quality of the results.

## REFERENCES


Amadei, G. Bernabini, M. Maino, A. & Orlando, L. 1978. Studio gravimetrico della bassa valle dei fiumi Sacco e Liri (Italia centrale). *Bollettino del Servizio Geologico d'Italia* XCIX: 19–28.

Bignardi, S. 2017. The uncertainty of estimating the thickness of soft sediments with the HVSR method: A computational point of view on weak lateral variations. *Journal of Applied Geophysics* 145: 28–38.

Boni, C. Bono, P. Di Filippo, M. Martelli, M.G. & Toro, B. 1982. Carta del tetto del potenziale serbatoio (Lazio sud-occidentale). *Contributo alla conoscenza delle potenzialità geotermiche della Toscana e del Lazio*. Roma.

Devoto, G. 1965. Lacustrine pleistocene in the lower Liri valley. *Geologia Romana* 4: 291–368.

Galli, P. Castenetto, S. & Peronace, E. 2012. The MCS macroseismic survey of the Emilia 2012 earthquakes. *Annals of Geophysics* 55(4).

Galli, P. Castenetto, S. & Peronace, E. 2017. The Macroseismic Intensity Distribution of the 30 October 2016 Earthquake in Central Italy (Mw 6.6): Seismotectonic Implications. *Tectonics* 36(10): 2179–2191.

Gosar, A. & Lenart, A. 2010. Mapping the thickness of sediments in the Ljubljana Moor basin (Slovenia) using microtremors. *Bulletin of Earthquake Engineering* 8(3): 501–518.

Ibs-von Seht, M. & Wohlenberg, J. 1999. Microtremor Measurements Used to Map Thickness of Soft Sediments. *Bulletin of the Seismological Society of America* 89(1): 250–259.

Lancia, M. Saroli, M. & Petitta, M. 2018. A Double Scale Methodology to Investigate Flow in Karst Fractured Media via Numerical Analysis: The Cassino Plain Case Study (Central Apennine, Italy). *Geofluids*: 1–12.

Molnar, S. Cassidy, J.F. Castellaro, S. Cornou, C. Crow, H. Hunter, J.A. Matsushima, S. Sánchez-Sesma, F.J. & Yong, A. 2018. Application of Microtremor Horizontal-to-Vertical Spectral Ratio (MHVSR) Analysis for Site Characterization: State of the Art. *Surveys in Geophysics* 39 (4): 613–631.

Nakamura, Y. 1989. A method for dynamic characteristics estimation of subsurface using microtremor on the ground surface. *Quarterly Report of the Railway Technical Reasearch Institute* 30: 25–33.

Oliver, M.A. & Webster, R. 2014. A tutorial guide to geostatistics: Computing and modelling variograms and kriging. *CATENA* 113: 56–69.

Pagliaroli, A. Avalle, A. Falcucci, E. Gori, S. & Galadini, F. 2015. Numerical and experimental evaluation of site effects at ridges characterized by complex geological setting. *Bulletin of Earthquake Engineering* 13(10): 2841–2865.

Rovida, A. Locati, M. Camassi, R. Lolli, B. & Gasperini, P. 2016. *CPTI15, the 2015 version of the Parametric Catalogue of Italian Earthquakes*.

Saroli, M. Lancia, M. Albano, M. Modoni, G. Moro, M. & Scarascia Mugnozza, G. 2014. New geological data on the Cassino intermontane basin, central Apennines, Italy. *Rendiconti Lincei* 25(2): 189–196.

Saroli, M. Lancia, M. & Petitta, M. 2016. The hydrogeology of the Cassino basin from Boni to Celico: 30 years later. *Rendiconti Online della Società Geologica Italiana* 40.

Saroli, M. & Moro, M. 2012. San Pietro Infine Basin. Field–trip guidebook. In: AIGeo (ed.), *16th Joint Geomorphological Meeting*. Rome.

SESAME 2004. Guidelines for the implementation of the H/V spectral ratio technique on ambient vibrations: measurements, processing, and interpretation. *SESAME European research project WP 12* D23.12.

Tertulliani, A. Arcoraci, L. Berardi, M. Bernardini, F. Camassi, R. Castellano, C. Del Mese, S. Ercolani, E. Graziani, L. Leschiutta, I. Rossi, A. & Vecchi, M. 2011. An application of EMS98 in a medium-sized city: The case of L'Aquila (Central Italy) after the April 6, 2009 Mw 6.3 earthquake. *Bulletin of Earthquake Engineering* 9(1): 67–80.

Trevisani, S. Boaga, J. Agostini, L. & Galgaro, A. 2017. Insights into bedrock surface morphology using low-cost passive seismic surveys and integrated geostatistical analysis. *Science of The Total Environment* 578: 186–202.